Load-estimation techniques for unsteady incompressible flows

Rival, David E.; Oudheusden, Bas van

DOI
10.1007/s00348-017-2304-3

Publication date
2017

Document Version
Final published version

Published in
Experiments in Fluids: experimental methods and their applications to fluid flow

Exp Fluids (2017) 58:20
DOI 10.1007/s00348-017-2304-3

RESEARCH ARTICLE

Load-estimation techniques for unsteady incompressible flows

David E. Rival[1] · Bas van Oudheusden[2]

Received: 10 June 2016 / Revised: 10 November 2016 / Accepted: 14 January 2017

Abstract In a large variety of fluid-dynamic problems, it is often impossible to directly measure the instantaneous aerodynamic or hydrodynamic forces on a moving body. Examples include studies of propulsion in nature, either with mechanical models or living animals, wings, and blades subjected to significant surface contamination, such as icing, sting blockage effects, etc. In these circumstances, load estimation from flow-field data provides an attractive alternative method, while at the same time providing insight into the relationship between unsteady loadings and their associated vortex-wake dynamics. Historically, classical control-volume techniques based on time-averaged measurements have been used to extract the mean forces. With the advent of high-speed imaging, and the rapid progress in time-resolved volumetric measurements, such as Tomo-PIV and 4D-PTV, it is becoming feasible to estimate the instantaneous forces on bodies of complex geometry and/or motion. For effective application under these conditions, a number of challenges still exist, including the near-body treatment of the acceleration field as well as the estimation of pressure on the outer surfaces of the control volume. Additional limitations in temporal and spatial resolutions, and their associated impact on the feasibility of the various approaches, are also discussed. Finally, as an outlook towards the development of future methodologies, the potential application of Lagrangian techniques is explored.

1 Introduction

We have come a long way since the pioneering work of Betz (1925) and Jones (1936), who introduced the methods, where pitot-rake wake surveys were used to extract the mean drag on a body of interest. Nearly a century later, and thanks to steady advances in high-speed imaging, simultaneous (time-resolved) volumetric velocimetry techniques, such as Tomographic PIV (Elsinga et al. 2006) and 4D-PTV (Schanz et al. 2016), are rapidly pushing the envelope, such that complete time-resolved data sets near or around a body of interest are becoming available. This opens up a myriad of possibilities in terms of data analysis, especially in the present context of non-intrusive load estimation: instantaneous aerodynamic loadings (either integral or sectional), fluid-structure interaction on moving bodies, complete characterization of natural swimmers and flyers, and so on. As a consequence of the limitations imposed by measurement capabilities, much of these analyses to date have been limited to two dimensions, time- or phase-averaged data sets, and an Eulerian framework, where cause-and-effect relationships can at times be difficult to infer. In contrast, Dabiri (2005) showed that with a Lagrangian framework, analogous wake vorticity and vortex added-mass terms could provide the instantaneous forces instead. This approach is elegant as it can elucidate how the forces from the wake are developed on the body, but to date is limited to our ability to obtain Lagrangian-like measurements, and will be discussed later in the review.

✉ David E. Rival
d.e.rival@queensu.ca

Bas van Oudheusden
b.w.vanoudheusden@tudelft.nl

[1] Department of Mechanical and Materials Engineering, Queen's University, Kingston, ON, Canada

[2] Department of Aerospace Engineering, Delft University of Technology, Delft, The Netherlands

Published online: 22 February 2017

In the following, a short review of the various approaches to extracting unsteady loads in incompressible flows will be provided from the point of view of their basic theoretical operating principles. These approaches range from the standard momentum-based approach, common to undergraduate texts, to the more elaborate vortex-based approaches reserved for a more expert user. Subsequently, a discussion of the practical challenges to implement these approaches in the actual experimental environment will be presented, where, for instance, temporal and spatial resolutions in turn have compounding effects on the uncertainty of the various approaches. Finally, the review will conclude with an outlook on the development of new, Lagrangian-based approaches, that not only offer potentially more accurate load estimations, but also further insight into the relationship between body shape, motion, and the ensuing wake downstream.

It should be stated here that this review serves to introduce the field, set the stage, and provide an outlook, by sketching the particular challenges that need to be addressed, rather than providing an in-depth and exhaustive assessment of the method capabilities. As the techniques (and measurement hardware) continue to evolve, we hope that this overview will encourage the community to undertake new studies that can be used to quantify uncertainty rigorously and in turn contrast the advantages of the various approaches against one other.

2 Methodology

2.1 Classical formulation

Let us start out with something as simple and yet extremely challenging as characterizing the forces on a landing bird, as depicted in Fig. 1. When focusing only on incompressible flows, we can start out with a generalized expression for the instantaneous force in a non-inertial reference frame:

$$\mathbf{F}(t) - \rho \iiint_{\mathrm{CV}} \mathbf{a}_{\mathbf{rel}} \mathrm{d}V = -\rho \iiint_{\mathrm{CV}} \frac{\partial \mathbf{u}}{\partial t} \mathrm{d}V - \rho \iint_{\mathrm{CS}} \mathbf{u}(\mathbf{u}_{\mathbf{rel}} \cdot \mathbf{n}) \mathrm{d}S - \iint_{\mathrm{CS}} p\mathbf{n} \mathrm{d}S + \iint_{\mathrm{CS}} (\overline{\overline{\tau}} \cdot \mathbf{n}) \mathrm{d}S, \tag{1}$$

where $\mathbf{n}$ is the normal vector to the control surface CS bounding control volume CV, and $\mathbf{a}$ ρ, $\mathbf{u}$, p, and $\overline{\overline{\tau}}$ represent acceleration, fluid density, velocity, pressure, and viscous stress, respectively. Note for this generalized case that both the acceleration and flux terms lie in a relative coordinate system so as to account for relative linear and angular acceleration effects. For sake of brevity, from here on in we will now focus on the force for an inertial control volume, which can be simplified into the following form:

$$\mathbf{F}(t) = -\rho \iiint_{\mathrm{CV}} \frac{\partial \mathbf{u}}{\partial t} \mathrm{d}V - \rho \iint_{\mathrm{CS}} \mathbf{u}(\mathbf{u} \cdot \mathbf{n}) \mathrm{d}S - \iint_{\mathrm{CS}} p\mathbf{n} \mathrm{d}S + \iint_{\mathrm{CS}} (\overline{\overline{\tau}} \cdot \mathbf{n}) \mathrm{d}S. \tag{2}$$

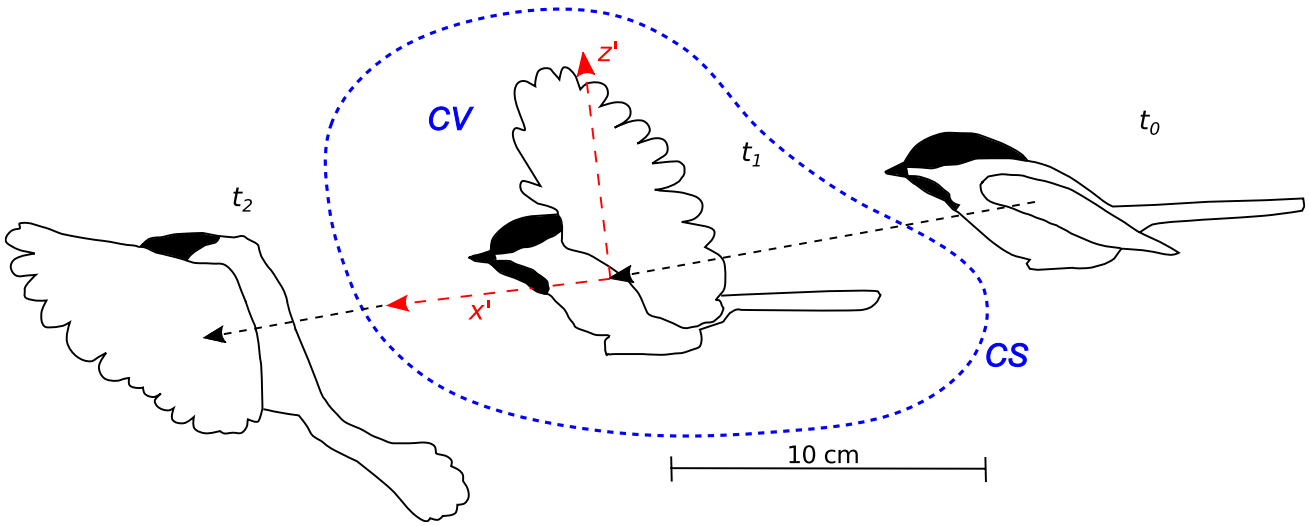

Fig. 1 Example of a chickadee coming into perch, showing (right-to-left) the end of the ballistic phase (t_0), the first frame, where the wrist is fully extended (t_1), and the final frame before the wrist flexes (t_2) ; adapted from Polet and Rival (2015). An arbitrarily-chosen control surface (CS) denoted in blue surrounds the control volume (CV) over which the instantaneous forces can be extracted at time step t_1

For a fixed control volume, the Leibnitz integral theorem can be applied to the unsteady term in Eq. (2):

$$-\rho \iiint_{\mathrm{CV}} \frac{\partial \mathbf{u}}{\partial t} \mathrm{d}V = -\rho \frac{\partial}{\partial t} \iiint_{\mathrm{CV}} \mathbf{u} \mathrm{d}V, \tag{3}$$

such that one can reformulate Eq. (2) in the following manner:

$$\mathbf{F}(t) = -\rho \frac{\partial}{\partial t} \iiint_{\mathrm{CV}} \mathbf{u} \mathrm{d}V - \rho \iint_{\mathrm{CS}} \mathbf{u}(\mathbf{u} \cdot \mathbf{n}) \mathrm{d}S - \iint_{\mathrm{CS}} p\mathbf{n} \mathrm{d}S + \iint_{\mathrm{CS}} (\bar{\bar{\tau}} \cdot \mathbf{n}) \mathrm{d}S. \tag{4}$$

The pressure distribution along each control surface can then be computed by integrating the Navier–Stokes equations from each corner of the control volume. Unal et al. (1997), Jardin et al. (2009), Rival et al. (2010), and Dabiri et al. (2013) have used this method to good success, although challenges with error propagation are rampant. Alternatively, if the complete velocity field within the control volume is accessible and boundary conditions that are known, the Poisson equation can be used to extract the pressure distribution instead, as performed by van Oudheusden et al. (2007), and then later reviewed in detail by van Oudheusden (2013). In some situations, the pressure relaxes quickly for a sufficient distance away from the body, such that this term can be neglected; however, it may be difficult to access *a priori* if this condition is satisfied. In fact, to maintain sufficient spatial resolution, the camera field of view is usually limited in size, and as such pressure is not likely to relax sufficiently so as to be ignored. One classic example, where the pressure was initially ignored, considered the thrust generation of a pitching foil (Koochesfahani 1989), and resulted in the mis-identification of the drag/thrust cross-over point. Many years later, the same problem was revisited, this time with the pressure term included (Bohl and Koochesfahani 2009), and not surprisingly a significant shift in the minimum frequency associated with thrust was observed.

Since the application of phase-averaged and time-resolved PIV, there have been a number of studies examining force estimation using a classic control-volume approach. In all these examples, pain-staking measures were taken to access the full velocity field around the body of interest using transparent models, complex optical techniques, etc. These studies include analyses by Unal et al. (1997), Kurtulus et al. (2007), Jardin et al. (2009), David et al. (2009), Rival et al. (2011), and Villegas and Diez (2014). To illustrate the full potential of the pressure and load determination technique, Fig. 2 reproduces some of the results of a study on a revolving low-aspect-ratio rectangular wing; see van de Meerendonk et al. (2016). Using phase-averaged tomographic-PIV on three partially overlapping volumes, the flow structure around the entire wing was captured for different phases of the motion. The pressure field around the wing and the spanwise distribution of the section lift and drag forces was subsequently evaluated in a non-inertial reference frame moving with the wing.

In certain circumstances, e.g., high-speed wind tunnels, time-resolved measurements are simply not possible. When only time-averaged velocity fields are available, as, for instance, was the case in the original study by Koochesfahani (1989), additional Reynolds-averaged terms that account for the intrinsic unsteadiness of the wake must be considered; see correction on original work in Bohl and Koochesfahani (2009). These specific Reynolds-averaged terms shown in Eq. (5) play an important role in such an analysis as they account for the implicit momentum fluctuations in the system. This methodology was originally presented in van Oudheusden et al. (2007) and has since also been successfully used by Gharali and Johnson (2014):

$$\overline{F_i} = -\rho \iint_{\mathrm{CS}} \bar{u}_i \bar{u}_j n_j \mathrm{d}S - \rho \iint_{\mathrm{CS}} \overline{u_i' u_j'} n_j \mathrm{d}S - \iint_{\mathrm{CS}} \bar{p} n_i \mathrm{d}S + \iint_{\mathrm{CS}} \mu \left(\frac{\partial \bar{u}_i}{\partial x_j} + \frac{\partial \bar{u}_j}{\partial x_i}\right) n_j \mathrm{d}S. \tag{5}$$

When dealing specifically with estimates of mean (steady) forces from phase-averaged data on periodic wakes, the net change in acceleration over the cycle is zero. This is naturally very convenient when, for instance, estimating mean lift and drag forces of flying animals in equilibrium conditions, e.g., Hubel et al. (2009) and Ben-Gida et al. (2013). When full time-resolved force estimation is required, and sufficient near-body acceleration data cannot be extracted, the natural next step is to work towards a so-called Derivative-Moment Transformation in which the volume integral is conveniently transformed into a surface integral, as detailed in the next section.

2.2 Derivative-moment transformation

Evaluation of the acceleration term as part of the overall aerodynamic loading requires complete time-resolved velocity measurements within the control volume. However, more often than not the body of interest blocks complete optical access via shadows and parallax effects. Furthermore, the laser often produces strong reflections near the object surface, where accelerations are highest, thus leading to large errors in the prediction of the acceleration term. For this reason, it is useful to transform the volume integral term in Eq. (4) into a surface integral. To achieve this transformation, one may expand the first term on the

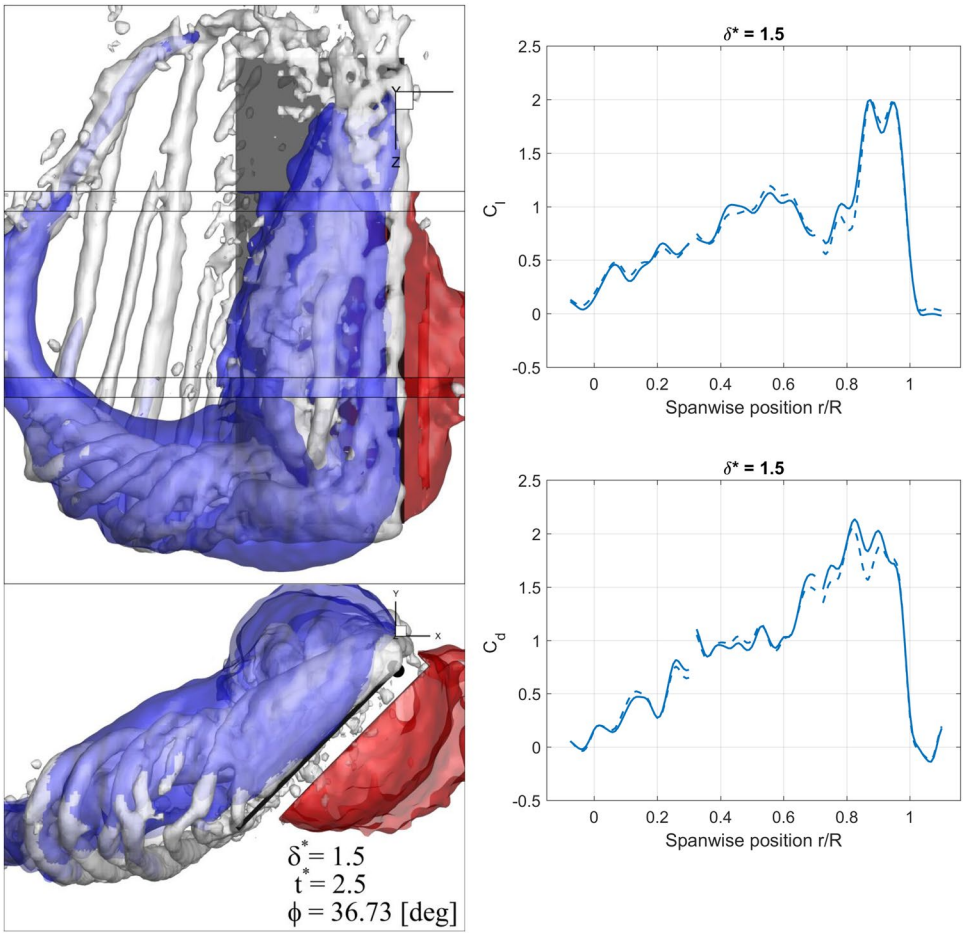

Fig. 2 Pressure and sectional load results for a revolving rigid wing. *Left* isosurfaces of Q-criterion ($Q = 3$) in *white* coloured by regions of high pressure (−13 Pa) in *red* and low pressure (6 Pa) in *blue*. *Right* spanwise distribution of the section lift (*top*) and drag (*bottom*). The *solid* and *dashed lines* represent changes in the interval between time steps, which affect the calculation of the acceleration term. *Bumps* in the curve represent shedding of vortex structures (see van de Meerendonk et al. (2016) for details on the reconstruction)

right-hand side of Eq. (4), as shown in Mohebbian and Rival (2012):

$$\mathbf{F}(t) = -\rho\frac{\partial}{\partial t}\iint_{CS}\mathbf{x}(\mathbf{u}\cdot\mathbf{n})\mathrm{d}S - \rho\iint_{CS}\mathbf{u}(\mathbf{u}\cdot\mathbf{n})\mathrm{d}S - \iint_{CS}p\mathbf{n}\mathrm{d}S + \iint_{CS}(\overline{\overline{\tau}}\cdot\mathbf{n})\mathrm{d}S, \tag{6}$$

where $\mathbf{x}$ is the position vector measured from any fixed frame of reference. This transformation is applied under the conditions that the velocity field is divergence free (incompressible flow) and that the body is thin, e.g., most lifting bodies. In contrast, contributions from thick (bluff) bodies must not be ignored, since an additional force term ($\mathbf{F}(t)_B$) accounting for the acceleration of the displaced body volume B must be accounted for

$$\mathbf{F}(t)_B = -\rho\frac{\partial}{\partial t}\iiint_{B}\mathbf{b}\mathrm{d}V, \tag{7}$$

where $\mathbf{b}$ represents the body velocity itself. This additional force simplifies to

$$\mathbf{F}(t)_B = -\rho B\frac{\partial\mathbf{b}}{\partial t}, \tag{8}$$

and eventually vanishes as the body volume shrinks to that of a thin plate or airfoil.

The Föppl transformation used above has been checked on synthetic cases by Wu et al. (2005), Minotti (2011), and Mohebbian and Rival (2012). Limitations regarding the size and proximity of the control surfaces relative to the body of interest, as well as the effect of vortical structures in the wake, have been examined in the latter paper. In Fig. 3, the positioning of four test control volumes relative to the accelerating plate are shown, while in Fig. 4, the effect of control-volume positioning on the impact of each term is characterized. One can observe that as one expands the control-volume size that the unsteady and convective contributions grow in scale. At the same time, the pressure term remains more or less constant, while the viscous term is always negligible. As discussed in the paper, there is little benefit to expanding the control-volume size, since the spatial resolution on the camera chip cannot be increased in most practical

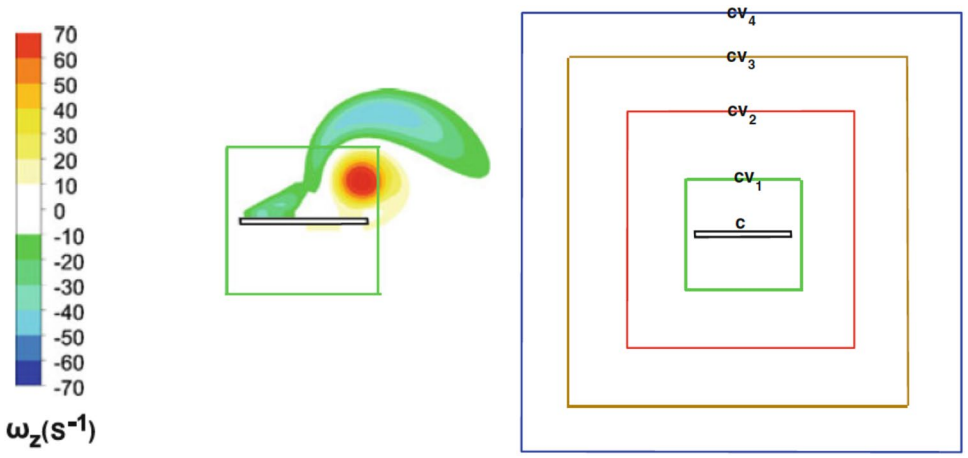

Fig. 3 Effect of control-volume size (relative positioning) has been tested for an accelerating plate with deep dynamic stall (*left*). Four control volumes were systematically tested on this synthetic test case; adapted from Mohebbian and Rival (2012)

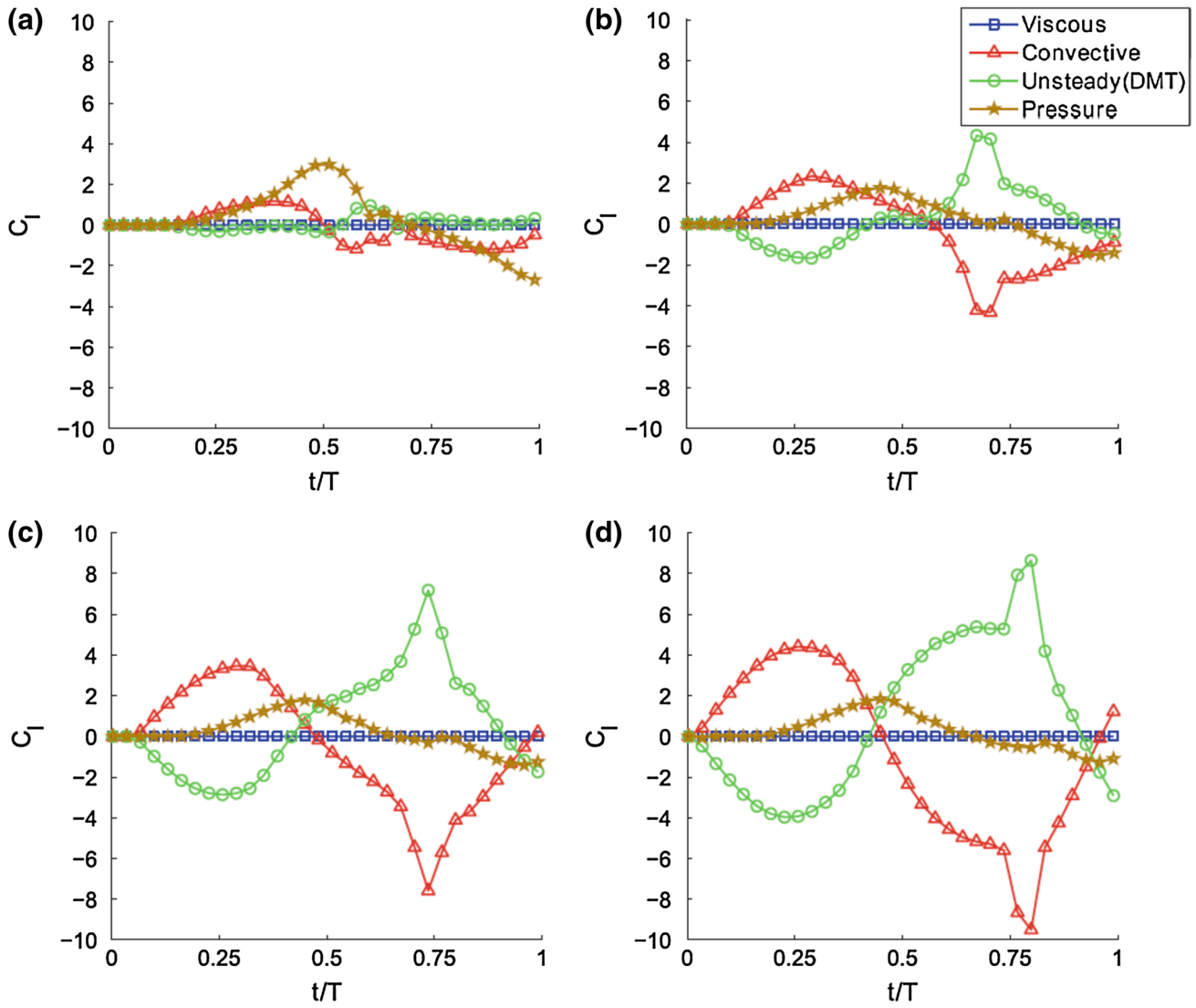

Fig. 4 In an example of estimating instantaneous lift, the relative contributions of each term in the derivative-moment transformation approach are broken down for increasing control-volume size from **a** to **d** [see Fig. 3 of relative CV positions (adapted from Mohebbian and Rival 2012)]

cases. Future developments in large camera chips for time-resolved measurements might help.

Recently, Lentink et al. (2015) were successful in developing a test chamber to measure the free-flying performance of birds based on this above transformation, and it is likely that this approach will be used further in characterizing the inherent unsteadiness of natural propulsion. It should be noted that this transformation to eliminate the necessity of measuring near the body has in fact been used extensively with the vorticity formulation. This formulation, which has received much attention for its elimination of the pressure term, will be considered next.

2.3 Vorticity formulations

In Noca et al. (1997, 1999), a control-volume procedure that eliminates the explicit use of the pressure term through the introduction of vorticity instead was developed and tested on both synthetic and experimental data. Among the various formulations detailed in Noca et al. (1999), the most appealing is the one that again converts the volume integral into a surface integral, shown here for a two-dimensional problem. Note that again additional contributions for thick bodies (Eq. 7) are ignored for sake of brevity:

$$\mathbf{F}(t) = \iint_{\mathrm{CS}} \mathbf{n}\gamma_{\mathrm{flux}}\mathrm{d}S, \tag{9}$$

where γ_{flux} is defined with the unit tensor $\mathbf{I}$ and viscous stress tensor $\overline{\tau}$ as follows:

$$\begin{aligned}\gamma_{\mathrm{flux}} = {} & \frac{1}{2}u^2\mathbf{I} + \mathbf{uu} - \frac{1}{2}\mathbf{u}(\mathbf{x}\times\boldsymbol{\omega}) + \frac{1}{2}\boldsymbol{\omega}(\mathbf{x}\times\mathbf{u}) \\ & - \frac{1}{2}\left[\left(\mathbf{x}\cdot\frac{\partial\mathbf{u}}{\partial t}\right) - \mathbf{x}\frac{\partial\mathbf{u}}{\partial t} + \frac{1}{2}\frac{\partial\mathbf{u}}{\partial t}\mathbf{x}\right] \\ & + \frac{1}{2}\left[\mathbf{x}\cdot\left(\nabla\cdot\overline{\overline{\tau}}\right)\mathbf{I} - \mathbf{x}\left(\nabla\cdot\overline{\overline{\tau}}\right)\right].\end{aligned} \tag{10}$$

Needless to say, the elegance of this particular formulation, since used in Ferreira et al. (2011), Sterenborg et al. (2013), DeVoria and Ringuette (2013), and DeVoria et al. (2014), allows for efficient force extraction without need for pressure estimates nor measurements near the body's surface. However, from Eq. (10), it is clearly seen that beyond the additional error amplification introduced by the spatial differentiation required to go from velocity to vorticity, several new terms are also introduced, thus compounding error. As with Eq. (6), one must also face the so-called *moment-arm dilemma* or noise amplification problem. Here, the positioning of the origin of x influences the local error, which is analogous to the choice of reference pressure location for the direct-pressure integration approach (see DeVoria et al. (2014) for a complete discussion).

When considering cases, where the far-field condition is irrotational, the classical unbounded approach, as described by Saffman (1992), can in principle be applied:

$$\mathbf{F} = \rho \iiint_{\infty} (\mathbf{u}\times\boldsymbol{\omega})\mathrm{d}V, \tag{11}$$

where again, we have ignored the contribution due to thick bodies, as this additional contribution is usually sufficiently small. As described above with Eq. 7, see Kriegseis and Rival (2014) for a discussion on how this term vanishes for airfoil shapes. Note that accurately capturing the vorticity field next to the body surface is a non-trivial challenge for the above expression. Let us consider the simple fact that, as described by Protas (2007), this above approach rapidly breaks down as vorticity advects away from the body of interest and across the control surface (field of view). To combat this limitation, Quartapelle and Napolitano (1983) developed a clever approach weighting vorticity closest to the body instead. Despite attempts to reformulate this approach by Protas (2007), complete information regarding the wall-bounded vorticity around the body of interest is required, thus making the approach impractical for most physical experiments. For some excellent reviews of these diverse vorticity-based methods, the reader is also directed to the works of Protas et al. (2000) and Graziani and Bassanini (2002).

With the advent of time-resolved volumetric measurement techniques coming online, such data sets now allow for a complete three-dimensional analysis of the instantaneous forces on three-dimensional bodies, as recently attempted for finite aspect ratio, accelerating plates in Kriegseis and Rival (2014), or for the vortex-ring wakes of fish in Mendelson and Techet (2015). This is akin to the methods proposed by Wu (1981) and Lighthill (1986), and tested on two-dimensional planes by Lin and Rockwell (1996) and Poelma et al. (2006). In instances when vorticity crosses the control surface in the far field, the instantaneous force determined in Eq. (11) can be reworked into two contributing terms (again for thin bodies) to avoid accounting for flux of vorticity in the wake, as described by Wu et al. (2006):

$$\mathbf{F} = -\rho\frac{d\mathbf{H}}{dt} + \rho \iiint_{\mathrm{CV}} (\mathbf{u}\times\boldsymbol{\omega})\mathrm{d}V, \tag{12}$$

where $\mathbf{H}$ is the hydrodynamic impulse and represents a mathematical proxy for the body surface vorticity contribution, such that

$$\mathbf{H} = \frac{1}{2}\iiint_{\mathrm{CV}} (\mathbf{x}\times\boldsymbol{\omega})\mathrm{d}V. \tag{13}$$

The second term in Eq. (12) is commonly referred to as the vortex force or Lamb vector, and as in Eq. (11) accounts for the wake development shedding off of the body surface in time. Provided a sufficiently large measurement volume can be used, this methodology is elegant in that identification of specific regions of force contribution, such as compact vortical structures, can be identified to provide deeper insight into the source of the aerodynamic loadings. However, limitations with spatial resolution for such measurements still hamper its application at higher Reynolds numbers and are the subject of the next section.

3 Practical considerations

As described above, an extensive set of force-extraction procedures have been developed and tested over the last decade. For the time-averaged characterization of aerodynamic loadings on an airfoil, as tested in van Oudheusden et al. (2007), it was found when varying the control-volume size that uncertainty in lift could be estimated to within 2%, whereas drag could only be resolved to within 20%, for attached-flow conditions. To date, no robust studies on uncertainty estimation have been performed for instantaneous force estimations with noisy data (be its classical, DMT, or with vorticity formulations). However, the short temporal discrepancies in estimates on the order of 10% observed in the synthetic test case of Mohebbian and Rival (2012) can be attributed to significant error propagation across the wake, as discussed by Kurtulus et al. (2007). These idealized results show that the discrepancies are strongest in the direction of drag due to the higher gradients of velocity across the rear control surface, associated with the crossing of wake vortices. These observed disparities in drag estimation warrant the development of future test cases to properly identify sources of error and associated limitations for realistic laboratory conditions, and across the variety of methods presented here.

When examining the general approaches described in Sects. 2.1, 2.2, and 2.3, we must take a careful look at the effect of error propagation on the overall accuracy of each force-extraction procedure. Despite the fact that Eqs. 4 and 6 require pressure explicitly and, therefore, must contend with challenges either from direct integration or through the Poisson equation, they both contain fewer terms, multiplications, and gradient operations, as shown in Table 1. In contrast, the uncertainty associated with extracting pressure directly (see van Oudheusden 2013), particularly when the control volume must remain relatively small relative to the body, as is often the case in the air with limited illumination, can be side-stepped with Eq. 9, as demonstrated by Noca et al. (1999). To date, no (systematic) comparative assessment has been published that shows definitively which of these approaches is more accurate or more robust under realistic experimental conditions. As such, it appears that the approach chosen is still much a matter of taste. The additional benefit of the classical formulation with pressure extraction is of course that also the pressure is evaluated explicitly, which can provide valuable insight in its own right.

The aerodynamic and hydrodynamic studies in consideration typically range from transitional up to fully-turbulent conditions, the latter being especially attractive for experimental investigations as computational costs soar. Since PIV measurements are inherently scalable that is to say that the field of view and inter-frame timing can be adjusted for the characteristic scales of the problem at hand, the dynamic spatial range and dynamic velocity range remain constant from one configuration to the next; see Adrian and Westerweel (2011). However, when considering the very nature of turbulent (three-dimensional) flows, appropriately-resolved volumetric reconstructions are necessary to account for the unsteady and flux terms over a control volume. As Reynolds numbers are increased, the limited dynamic range of PIV becomes a bottleneck, in turn making high-density Lagrangian approaches, such as 4D-PTV more attractive. Although the contribution of three dimensionality and spatial/temporal resolution has not been explored in the context of force estimation, its influence has been characterized when extracting pressure, which too plays a significant role in the classical and Derivative-Moment Transformation formulations. In the work by Violato et al. (2011), the relative contribution of these three-dimensional terms was found to contribute to errors as high as 20% when estimating the material derivative and pressure gradient fields in an otherwise bulk two-dimensional flow. In general, there is a case to be made that the larger energy-containing scales will be most critical in estimating all terms in the force decomposition (in contrast to isotropic

Table 1 Overview of potential error source for the three standard force-extraction techniques

Method	No. terms	No. multiplications	No temporal derivatives	No gradient operations	Pressure term?
Classical formulation (with Poisson)	4	2	2	3	Yes
Derivative-moment transformation method (with Poisson)	4	3	2	3	Yes
Vorticity formulation (Noca et al. 1999)	9	13	2	6	No

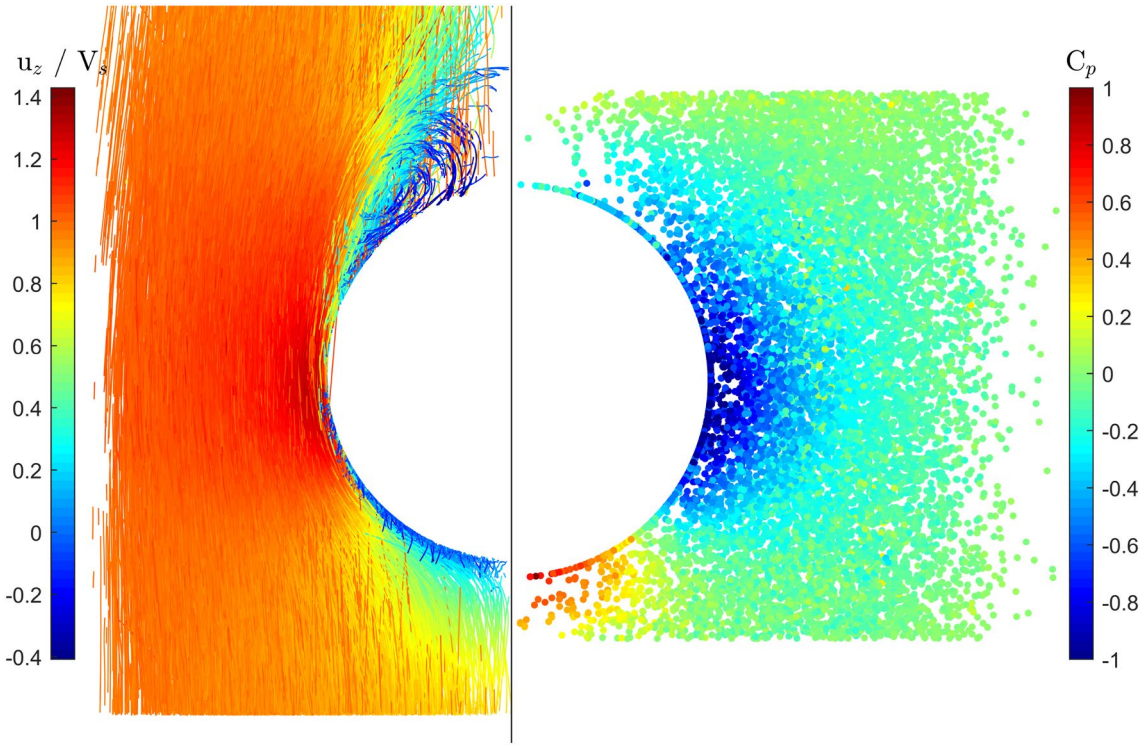

Fig. 5 Example of a recent instantaneous 4D-PTV reconstruction for a falling, optically-matched sphere (*left*). Tracks are coloured by relative velocity normalized with the settling velocity (u_z/V_s). Only a relatively sparse selection of the total number of tracks is shown for clarity. On the *right*, an instantaneous description of pressure (pressure coefficient) has been retrieved on the tracked particles themselves, adapted from Neeteson et al. (2016)

behaviour at smaller scales), but to date, no concrete evidence exists to support these assumptions. Therefore, further test cases, or even synthetic data sets, will be required to quantify these sources of error going forward.

In fact, despite the commonality between many of the experiments discussed in this review, seldom is the implementation issues presented in much detail. The most immediate constraints can be attributed to limited spatial and temporal resolutions associated with the cameras and illumination (e.g., laser power), for which rapid leaps in performance can no longer to be expected. Testing in water versus air has its inherent advantages from the perspective of a stronger signal-to-noise ratio as well as a potentially finer temporal resolution (similar Reynolds numbers can be achieved at slower physical time scales). For this reason, a large proportion of highly unsteady aerodynamic problems are studied in water rather than air. Despite this inherent advantage in the temporal resolution, problems involving fluid-structure interaction do not scale easily from air to water unless great lengths are taken with techniques, such as *cyber-physical fluid dynamics*, e.g., Mackowski and Williamson (2011) and Onoue and Breuer (2016). Furthermore, particle images in water are generally larger, such that PIV recordings will have a finer spatial resolution in the air, which is critical for capturing, for instance, regions of shear crossing control surfaces; see Mohebbian and Rival (2012). As discussed by Kähler et al. (2012a), the spatial resolution of PIV is limited by seeding particle size (and therefore inter-particle spacing), such that the only substantial measure to increase resolution in such unsteady force estimates is in fact to move towards Lagrangian particle tracking, as will now be discussed in the outlook section in the following.

4 Outlook

Currently, all approaches discussed above are implemented using an Eulerian framework acquired through the standard planar or volumetric PIV measurement techniques. In some cases, the limitations with regard to spatial resolution in terms of discretization in regions of high shear or near walls poses a significant challenge, as described by Westerweel (2008) and Kähler et al. (2012b), respectively. The following describes a prospective outlook towards the implementation of Lagrangian-based measurement techniques and analyses going forward.

Up until very recently, PTV measurements have been limited to relatively low seeding densities, thus

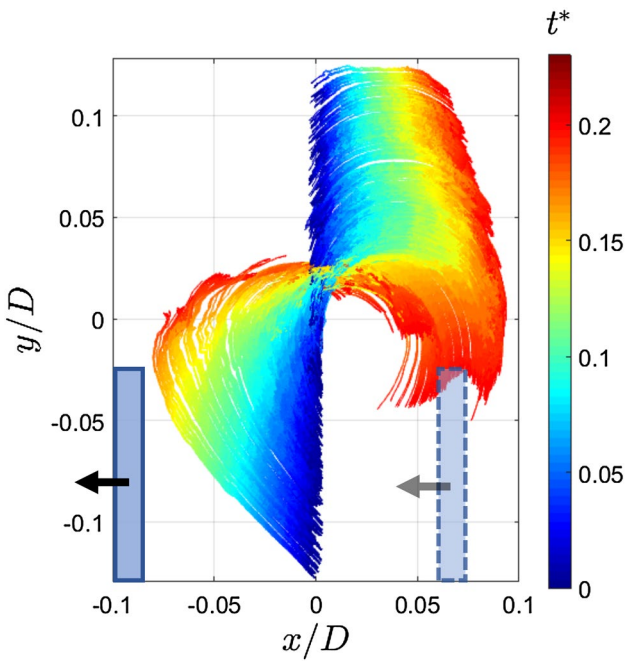

Fig. 6 Pathlines emanating from a arbitrarily-chosen starting plane ($x/d = 0$) coloured in normalized time ($t^* = tU/d$), where U is the plate velocity and d is plate diameter. Note for this test case, the plate is accelerating; see Fernando and Rival (2016) for details on the experiment

prohibiting its use for classical force estimation or wake-vortex volume extraction discussed in the following. However, this new so-called 4D-PTV or *Shake-The-Box* approach that allows significant particle densities to be tracked has opened up a whole new gamut of possibilities; see Schanz et al. (2016). Unlike existing Eulerian-based imaging techniques, such as Tomo-PIV, this new approach provides detailed Lagrangian tracking information (long pathlines) at ultra-high seeding densities, on the order of 100,000 tracked particles per time step. Before we look at the full potential of Lagrangian data, we can start by already identifying a considerable advantage with 4D-PTV data with the increase in dynamic spatial resolution when compared to classical correlation-based approaches; see Kähler et al. (2012a) for a quantitative comparison showing the virtues of PTV versus PIV measurements. As an example of what these 4D-PTV data sets just might look like, Fig. 5 (left) describes a simple test case with a falling (optically-matched) sphere. Here, the dense track information allows for the identification of an emerging wake with higher resolution than Eulerian reconstructions. In parallel, Fig. 5 (right) demonstrates our ability to simultaneously perform pressure extraction using tesselated networks (Neeteson et al. 2016), which further aids in the application of classical force-extraction approaches with higher spatial resolution. Note though that an analogous compromise between sufficient spatial resolution and imaging field of view still remains, as with the classical approach.

However, the real strength in Lagrangian data sets is the inherent temporal information, e.g., pathline reconstructions. Here, we discuss the possibility of using Lagrangian-based measurements to identify vortex added mass, as has been proposed by Dabiri (2005). Based on the classical concept of a *drift volume* (Ω_d), which was originally developed by Darwin (1953), and provides a direct measure of the body added-mass ($m_a = \rho\Omega_d$), Dabiri (2005) presented the following expression as a means to estimate the instantaneous loading:

$$\mathbf{F}(t) = \rho\frac{\partial}{\partial t}\iiint_{\mathrm{CV}}(\mathbf{x}\times\boldsymbol{\omega})\mathrm{d}V + \rho c_{ii}\frac{\partial}{\partial t}(\Omega_V\mathbf{u}_{Vi}), \tag{14}$$

where the second term, the *wake-vortex added mass*, contains an added-mass coefficient c_{ii}, a wake-vortex volume Ω_V, and a wake-vortex velocity $\mathbf{u}_{Vi}$ relative to the body in the ith direction. The elegance of this approach, albeit suggested more than a decade before 4D-PTV measurements were even possible—see Schanz et al. (2016)—is that wake-vortex volumes can now be extracted directly using the drift-volume concept developed by Darwin (1953) more than sixty years ago. At the time of publication Dabiri (2005), only had planar PIV measurement techniques at their disposal, for which wake-vortex volume identification was limited to calculations from finite-time Lyapunov exponents (Haller 2002), and thus required an assumption of projecting three-dimensional wake information onto a two-dimensional plane. Although application of this technique to 4D-PTV data is ongoing, initial estimates of a drift volume for a canonical accelerating plate are presented in Figs. 6 and 7. Here, a circular plate is accelerated from rest and experiences a rapid spike and relaxation in drag through a complex process of vortex-ring formation and pinch off; see Fernando and Rival (2016) for details about the experimental setup. In Fig. 6, we can observe pathlines emanating from an arbitrarily-chosen starting plane ($x/d = 0$), whereas in Fig. 7, the drift volume can be estimated by tracking individual particles relative to the starting plane (volume encapsulated by red and green tagging). The application and validation of drift-volume measurements are still very much at its infancy, but a large push in this direction is expected in the coming years now that the high-density, Lagrangian measurement techniques are finally available.

Therefore, to conclude this brief review with a look to the future, it is proposed that for a variety of applications, the community will gradually embrace Lagrangian-type measurements, such as 4D-PTV. These Lagrangian data sets will potentially provide higher accuracy

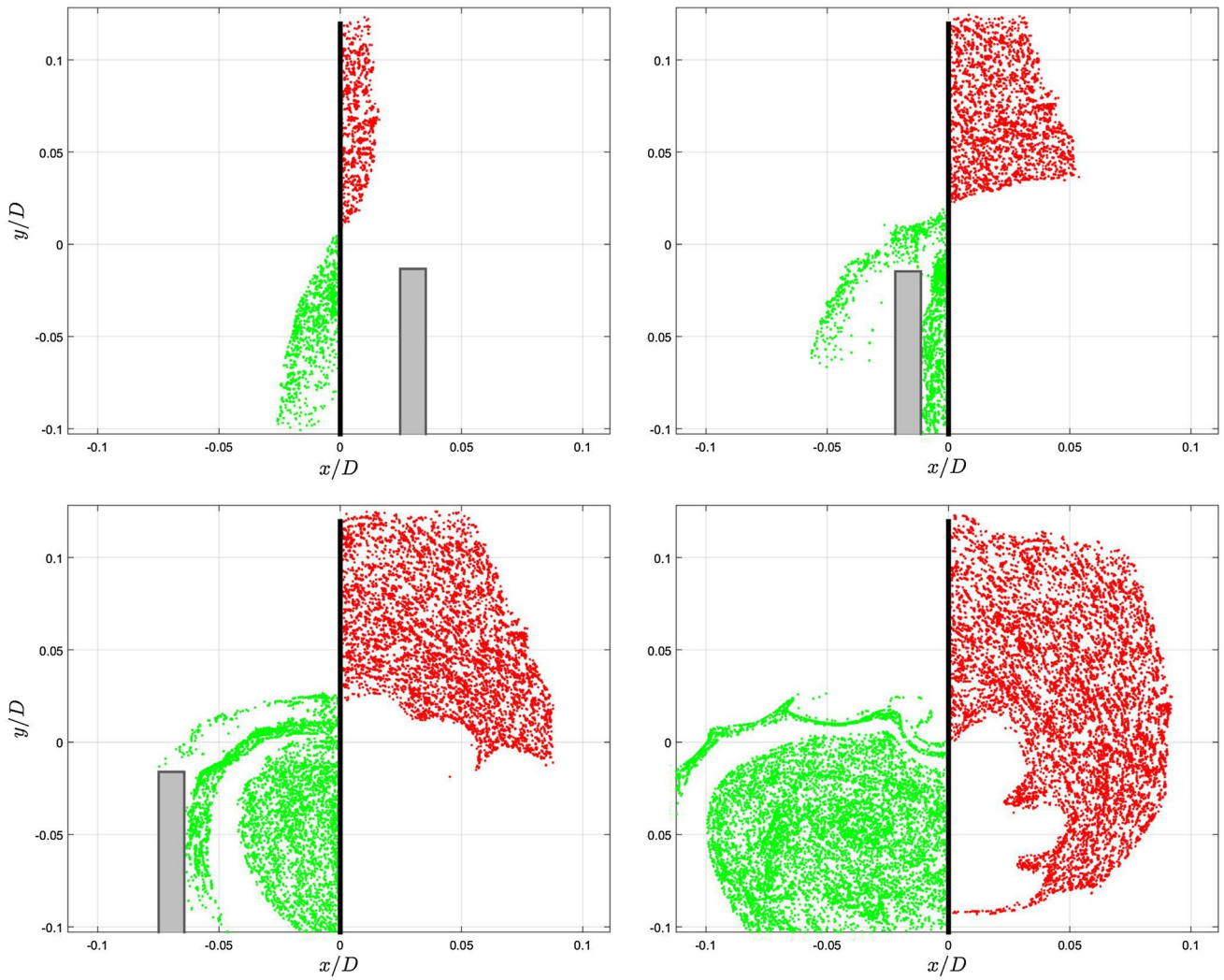

Fig. 7 Example of a drift-volume estimation on an accelerating circular plate. The positive (*green*) and negative (*red*) drift volumes are shown for four linearly-spaced time steps: $t^* = 0.085$ (*upper left*), $t^* = 0.170$ (*upper right*), $t^* = 0.225$ (*bottom left*), $t^* = 0.340$ (*bottom right*). Note that the starting plane's position (*black line*) is arbitrarily chosen

in instantaneous load estimation, either using classical approaches or ones with drift-volume estimates, and further will also allow for complimentary understanding of topological features (Huang and Green 2015) by connecting sources of vorticity production on a body to its wake. Undoubtedly there remains much work in the development and validation of these Lagrangian-based analyses, and in turn, it is hoped that with access to new high-density Lagrangian tracking, we will further uncover the salient mechanisms of this broad class of unsteady flows.

References

Adrian RJ, Westerweel J (2011) Particle image velocimetry. Cambridge University Press

Ben-Gida H, Kirchhefer A, Taylor ZJ, Bezner-Kerr W, Guglielmo CG, Kopp GA, Gurka R (2013) Estimation of unsteady aerodynamics in the wake of a freely flying european starling (sturnus vulgaris). PLOS One 8(11):e80086

Betz A (1925) A method for the direct determination of profile drag (in German). Zeitschrift für Flugtechnik und Motorluftschifffahrt 16:42–44

Bohl DG, Koochesfahani MM (2009) MTV measurements of the vortical field in the wake of an airfoil oscillating at high reduced frequency. J Fluid Mech 620:63–88

Dabiri JO (2005) On the estimation of swimming and flying forces from wake measurements. J Exp Biol 208:3519–3532

Dabiri JO, Bose S, Gemmell BJ, Colin SP, Costello JH (2013) An algorithm to estimate unsteady and quasi-steady pressure fields from velocity field measurements. J Exp Biol 217:331–336

Darwin CG (1953) Note on hydrodynamics. Math Proc Cambridge Philos Soc 49(2):342–354

David L, Jardin T, Farcy A (2009) On the non-intrusive evaluation of fluid forces with the momentum equation approach. Measure Sci Technol 20:095401

DeVoria AC, Ringuette M (2013) On the flow generated on the leeward face of a rotating flat plate. Exp Fluids 54:1495

DeVoria ACJ, Carr ZR, Ringuette MJ (2014) On calculating forces from the flow field with application to experimental volume data. J Fluid Mech 749:297–319

Elsinga GE, Scarano F, Wieneke B, van Oudheusden BW (2006) Tomographic Particle Image Velocimetry. Exp Fluids 41:933–947

Fernando JFF, Rival DE (2016) Reynolds-number scaling of vortex pinch-o on low-aspect-ratio propulsors. J Fluid Mech 799:R3

Ferreira CJS, van Bussel GJW, van Kuik GAM, Scarano F (2011) On the use of velocity data for load estimation of a vawt in dynamic stall. J Solar Energy Eng 133:011006

Gharali K, Johnson DA (2014) Piv-based load investigation in dynamic stall for different reduced frequencies. Exp Fluids 54:1–14

Graziani G, Bassanini P (2002) Unsteady viscous flows about bodies: Vorticity release and forces. Meccanica 37:283–303

Haller G (2002) Lagrangian coherent structures from approximate velocity data. Phys Fluids 14(6):1851–1861

Huang Y, Green MA (2015) Detection and tracking of vortex phenomena using lagrangian coherent structures. Exp Fluids 56:147

Hubel TY, Hristov NI, Swartz SM, Breuer KS (2009) Time-resolved wake structure and kinematics of bat flight. Exp Fluids 46:933–943

Jardin T, Chatellier L, Farcy A, David L (2009) Correlation between vortex structures and unsteady loads for flapping motion in hover. Exp Fluids 47:655–664

Jones BM (1936) Measurement of profile drag by the pitot-traverse method. ARC R&M No. 1688

Kähler CJ, Scharnowski S, Cierpka C (2012a) On the resolution limit of digital particle image velocimetry. Exp Fluids 52(6):1629–1639

Kähler CJ, Scharnowski S, Cierpka C (2012b) On the uncertainty of digital PIV and PTV near walls. Exp Fluids 52(6):1641–1656

Koochesfahani MM (1989) Vortical patterns in the wake of an oscillating airfoil. AIAA J 27:1200–1205

Kriegseis J, Rival D (2014) Vortex force decomposition in the tip region of impulsively-started flat plates. J Fluid Mech 756:758–770

Kurtulus DF, Scarano F, David L (2007) Unsteady aerodynamics force estimation on a square cylinder by TR-PIV. Exp Fluids 42:185–196

Lentink D, Haselsteiner AF, Ingersoll R (2015) In vivo recording of aerodynamic force with an aerodynamic force platform: from drones to birds. J R Soc Interface 12:20141283

Lighthill MJ (1986) Fundamentals concerning wave loading on offshore structures. J Fluid Mech 173:667–681

Lin J-C, Rockwell D (1996) Force identification by vorticity fields: techniques based on flow imaging. J Fluids Struct 10:663–668

Mackowski AW, Williamson CHK (2011) Developing a cyber-physical fluid dynamics facility for fluid-structure interaction studies. J Fluids Struct 27:748–757

Mendelson L, Techet AH (2015) Quantitative wake analysis of a freely swimming fish using 3D synthetic aperture PIV. Exp Fluids 56:135

Minotti FO (2011) Determination of the instantaneous forces on flapping wings from a localized fluid velocity field. Phys Fluids s1-9(1):91–93

Mohebbian A, Rival D (2012) Assessment of the derivative-moment transformation method for unsteady-load estimation. Exp Fluids 53:319–330

Neeteson NJ, Bhattacharya S, Rival DE, Michaelis D, Schanz D, Schroeder A (2016) Pressure-field extraction from Lagrangian flow measurements: first experiences with 4D-PTV data. Exp Fluids 57:102

Noca F, Shiels D, Jeon D (1997) Measuring instantaneous fluid dynamic forces on bodies, using only velocity fields and their derivatives. J Fluids Struct 11:345–350

Noca F, Shiels D, Jeon D (1999) A comparison of methods for evaluating time-dependent fluid dynamic forces on bodies, using only velocity fields and their derivatives. J Fluids Struct 13:551–578

Onoue K, Breuer KS (2016) Vortex formation and shedding from a cyber-physical pitching plate. J Fluid Mech 793:229–247

Poelma C, Dickson WB, Dickinson MH (2006) Time-resolved reconstruction of the full velocity field around a dynamically-scaled flapping wing. Exp Fluids 41:213–225

Polet DT, Rival DE (2015) Rapid area change in pitch-up manoeuvres of small perching birds. Bioinsp Biomimet 10(1):066004

Protas B (2007) On an attempt to simplify the Quartapelle Napolitano approach to computation of hydrodynamic forces in open flows. J Fluids Struct 23:1207–1214

Protas B, Styczek A, Nowakowski A (2000) An effective approach to computation of forces in viscous incompressible flows. J Comput Phys 159:231–245

Quartapelle L, Napolitano M (1983) Force and moment in incompressible flows. AIAA J 21:911–913

Rival DE, Manejev R, Tropea C (2010) Measurement of parallel blade-vortex interaction at low Reynolds numbers. Exp Fluids 49:89–99

Rival DE, Schoenweitz D, Tropea C (2011) Vortex interaction of tandem pitching and plunging plates: a two-dimensional model of hovering dragonfly-like flight. Bioinspir Biomimet 6(1):016008

Saffman P (1992) Vortex Dynamics. Cambridge Monographs on Mechanics and Applied Mathematics. Cambridge University Press

Schanz D, Gesemann S, Schroeder A (2016) Shake The Box: Lagrangian particle tracking at high particle image densities. Exp Fluids 57-70

Sterenborg JJHM, Lindeboom RCJ, Ferreira CJS, van Zuijlen AH, Bijl H (2013) Assessment of piv-based unsteady load determination of an airfoil with actuated flap. J Fluids Struct 45:79–95

Unal M, Lin J-C, Rockwell D (1997) Force prediction by PIV imaging: a momentum-based approach. J Fluids Struct 11:965–971

van de Meerendonk R, Percin M, van Oudheusden B (2016) Three-dimensional flow and load characteristics of flexible revolving wings at low Reynolds number. In: 18th International Symposium on Applications of Laser Techniques to Fluid Mechanics, 4–7 July, Lisbon, Portugal

van Oudheusden BW (2013) PIV-based pressure measurement. Measure Sci Technol 24(032001):1–32

van Oudheusden BW, Scarano F, Roosenboom EWM, Casimiri EWF, Souverein LJ (2007) Evaluation of integral forces and pressure fields from planar velocimetry data for incompressible and compressible flows. Exp Fluids 43(2–3):153–162

Villegas A, Diez F (2014) Evaluation of unsteady pressure fields and forces in rotating airfoils from time-resolved piv. Exp Fluids 55:1697

Violato D, Moore P, Scarano F (2011) Lagrangian and Eulerian pressure field evaluation of rod-airfoil flow from time-resolved tomographic PIV. Exp Fluids 50:1057–1070

Westerweel J (2008) On velocity gradients in PIV interrogation. Exp Fluids 44:831–842

Wu JC (1981) Theory for aerodynamic force and moment in viscous flows. AIAA J 19:432–441

Wu J-Z, Ma H-Y, Zhou J-Z (2006) Vorticity and vortex dynamics. Lecture notes in mathematics. Springer, Berlin Heidelberg

Wu J-Z, Pan Z-L, Lu X-Y (2005) Unsteady fluid-dynamic force solely in terms of control-surface integral. Phys Fluids 17:098102